

Transference number in polymer electrolytes: mind the reference-frame gap

Yunqi Shao, Harish Gudla, Daniel Brandell, and Chao Zhang*

Department of Chemistry-Ångström Laboratory, Uppsala University, Lägerhyddsvägen 1, P. O. Box 538, 75121 Uppsala, Sweden

Received March 4, 2022; E-mail: chao.zhang@kemi.uu.se

Abstract: The transport coefficients, in particular the transference number, of electrolyte solutions are important design parameters for electrochemical energy storage devices. Recent observation of negative transference numbers in PEO–LiTFSI under certain conditions has generated much discussion about its molecular origins, by both experimental and theoretical means. However, one overlooked factor in these efforts is the importance of the reference frame (RF). This creates a non-negligible gap when comparing experiment and simulation, because the fluxes in the experimental measurements of transport coefficients and in the linear response theory used in the molecular dynamics simulation are defined in different RFs. In this work, we show that by applying a proper RF transformation, a much improved agreement between experimental and simulation results can be achieved. Moreover, it is revealed that the anion mass and the anion-anion correlation, rather than ion aggregates, play a crucial role for the reported negative transference numbers.

One factor that limits the fast charging and discharging of lithium and lithium-ion batteries is the build-up of a salt concentration gradient in the cell during operation,^{1,2} since the anion flux due to migration must be countered by that of diffusion at steady state. It is therefore desirable for the electrolyte material to carry a greater fraction of cation for migration, so as to minimize the concentration gradient. This fraction, known as the cation transference number, is thus of vital importance in the search for novel electrolyte materials. It is therefore problematic that conventional liquid electrolytes display rather low such numbers, and even more troublesome that they are even lower for solid-state polymer electrolytes based on polyethers.

While the condition of a uniform concentration when measuring the transference number can be achieved in typical aqueous electrolytes, its experimental determination in polymer electrolytes is much more challenging, due to the continuous growth of the diffusion layer.³ At low concentration, the effect of the concentration gradient may be estimated by assuming an ideal solution without ion-ion interactions, as is done in the Bruce-Vincent method.⁴ At higher concentrations, its effect on the transference number can be taken into account by the concentrated solution theory developed by Newman, and obtained through a combination of experimental measurements.⁵

The cation transference number t_+^0 measured in these experiments is defined typically in the solvent-fixed reference frame (RF), denoted by the superscript 0 here.⁶ However, the transference number t_+^M as computed in molecular dynamics (MD) simulation based on the linear response theory,⁷ is instead related to the velocity correlation functions under the barycentric RF (denoted by the superscript M).

This difference creates a conceptual gap when comparing experiments and simulations, and to interpret results measured in different types of experiments, when seeking the molecular origin behind the observed phenomenon.

To illustrate this point, we here study a typical polymer electrolyte system: PEO–LiTFSI. For this, negative t_+^0 has been reported with Newman’s approach,^{8,9} which has rendered much discussion in the literature.^{10–12} While the formation of ion aggregates has often been suggested to cause such negative t_+^0 ,¹¹ only marginally negative values were observed in MD simulations,¹³ even when the correlation due to charged ion clusters was considered explicitly.

To reconcile these observations, we will first investigate how the choice of RF affect the transference number. In fact, it is possible to relate t_+^M to t_+^0 via a simple transformation rule, as shown by Woolf and Harris:¹⁴

$$\omega_0 t_+^0 = t_+^M - \omega_- \quad (1)$$

where the mass fraction of species i is denoted as ω_i . According to Eq. 1, the relation between t_+^0 and t_+^M depends only on the composition, specifically the mass fractions, of the electrolyte.

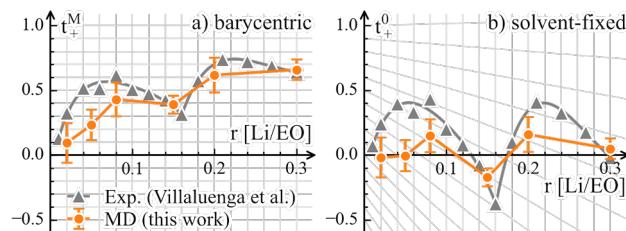


Figure 1. The transference number under a) barycentric RF and b) solvent-fixed RF in PEO–LiTFSI for different concentrations r [Li/EO] (the ratio of Li:ether oxygen). The conversion rule of t_+^M as determined by Eq. 1 is shown by projecting the grid of a) to b). The experimental data and fitting of t_+^0 are reproduced from Ref. 8. The transfer number in MD simulations are computed from the corresponding Onsager coefficients using Eq. 3, see the Supporting Information for simulation details.

While the two transference numbers are equivalent at the limit of infinite dilution ($\omega_0 \rightarrow 1$), they become distinctly different at higher concentration. As shown in Fig. 1, at the concentration where negative t_+^0 is observed, t_+^M is still positive. Moreover, t_+ generally shifts downward in the solvent-fixed RF as the concentration increases, as seen in Fig. 1. This trend can be expected, since at the other limit ($\omega_0 \rightarrow 0$), t_+^M must converge to the ω_- in order to satisfy Eq. 1. This suggests that t_+^0 will become increasingly sensitive at higher concentration since its value will be determined by the motion of a small fraction of solvent molecules.

The distinction between t_+^M and t_+^0 may already explain why negative transference number is seldom observed in MD simulations, where the barycentric RF is the default setting.

But more importantly, the strong dependency of t_+ on the RF suggests that the intuitive explanation of the observed negative t_+ being due to the population of ion aggregates is not necessarily the case. Instead, as pointed out in recent studies,^{15–19} the explicit consideration of ion-ion correlations is essential to understand ion transport in polymer electrolytes.

In the following, we will show how the ion-ion correlations contribute to the negative transference number in light of the RF. In the Onsager phenomenological equations,²⁰ the flux \mathbf{J}_i^S of species under a reference frame S can be considered as the linear response of the external driving forces \mathbf{X}_j acting on any species j :

$$\mathbf{J}_i^S = \sum_j \Omega_{ij}^S \mathbf{X}_j \quad (2)$$

where Ω_{ij}^S are the Onsager coefficients. For the index j , here we denote the solvent as 0, the cation as +, and the anion as -. In addition, the fluxes satisfy the following RF condition $\sum_i a_i^S \mathbf{J}_i^S = 0$, where a_i^S are the proper weighing factors, i.e. $a_i^M = M_i$ for the barycentric RF and $a_i^0 = \delta_{i0}$ for the solvent-fixed RF. Then, a unique set of the Onsager coefficients can be determined by applying the Onsager reciprocal relation: $\Omega_{ij}^S = \Omega_{ji}^S$, and the RF constraint $\sum_i a_i^S \Omega_{ij}^S = 0 \forall j$.

Knowing these Onsager coefficients, one can express the transport properties of interest here, i.e. the transference number and the ionic conductivity, as:

$$t_i^S = \frac{\sum_j q_i q_j \Omega_{ij}^S}{\sum_{j,k} q_j q_k \Omega_{jk}^S} \quad (3)$$

$$\sigma = \sum_{i,j} q_i q_j N_A^2 \Omega_{ij}^S \quad (4)$$

where q_i is the formal charge of i and N_A is the Avogadro constant. It is worth noting that unlike the transference number, the ionic conductivity is RF-independent because of the charge neutrality condition.

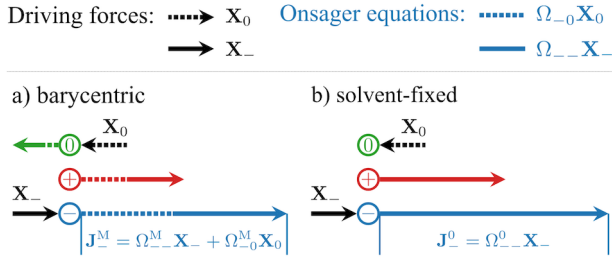


Figure 2. An illustration of the transformation procedure when converting Ω_{ij}^M to Ω_{ij}^0 for the case where the driving force acting on cation is zero. The dashed lines indicate relevant parts related to the solvent.

While the transformation of t_+ from the solvent-fixed RF to the barycentric RF can follow the straightforward rule of Eq. 1, the corresponding RF transformation of Ω_{ij} is not trivial. This is illustrated by a simplified example shown in Fig 2, where driving force acting on the cation is assumed to be zero. In the barycentric RF both driving forces \mathbf{X}_0 acting on solvent and \mathbf{X}_- acting on anion will contribute to the anion flux \mathbf{J}_-^M . When transforming the Onsager coefficients to the solvent-fixed RF, only the driving force \mathbf{X}_- contributes to the anion flux \mathbf{J}_-^0 , as $\Omega_{-0}^0 = 0$ by construction.

Nevertheless, the general transformation rule can be derived using the independent fluxes and driving forces,²¹ which is consistent with the above constructions. Following the notation of Miller,²² one can consider only the $n-1$ independent fluxes and driving forces in a n component system, where the flux of the solvent \mathbf{J}_0 is treated as a redundant variable. This leads to the following set of rules for the RF transformation:

$$A_{ij}^{RS} = \delta_{ij} + \frac{c_i}{\sum_k a_k^R c_k} \left(\frac{a_0^R a_j^S}{a_0^S} - a_j^R \right) \quad (5)$$

$$\mathbf{J}_i^R = \sum_{j \neq 0} A_{ij}^{RS} \mathbf{J}_j^S \quad (6)$$

$$\Omega_{ij}^R = \sum_{k,l \neq 0} A_{ik}^{RS} \Omega_{kl}^S A_{jl}^{RS} \quad (7)$$

where A_{ij}^{RS} is the matrix that converts the independent fluxes from the reference frame S to R and c_i is the molar concentration of species i . The coefficients Ω_{i0}^R may then be fixed according to the RF constraint. The specific transformation equations for the barycentric and solvent-fixed RFs are provided in the Supporting Information.

This transformation provides the connection between Ω_{ij}^0 measured experimentally and Ω_{ij}^M derived from MD simulations. Thus, one can compare Onsager coefficients under a common RF to see whether the simulation describes the same transport mechanism as in experiment or not. Here we computed Onsager coefficients following Miller’s derivation,⁶ with experimental measurements by Villaluenga et al.⁸ MD simulations were performed using GROMACS²³ and the General AMBER Force Field,²⁴ from which Onsager coefficients were derived with an in-house analysis software. Details of the conversion and simulation procedure can be found in the Supporting Information. In addition, we shall note here that an alternative set of transport coefficients, i.e. the Maxwell-Stefan diffusion coefficients, were originally reported from experiment,⁸ and they are consistent with the present framework (see the Supporting Information for the inter-conversion). However, the Onsager coefficients are favoured here because they are well-behaved at any given concentration and therefore helpful to understand the RF dependency of the ion-ion correlations.

As shown in Fig. 3, the conductivity and Onsager coefficients obtained from MD simulations generally matches the experimental values. In particular, Ω_{+-}^M is negative in the entire concentration range and this indicates an anti-correlation between cations and anions. Furthermore, we see that the experimentally observed negative transference number at $r = 0.15$ is reproduced in the MD simulation, with consistent features of Ω_{ij} , namely, $\Omega_{--}^0 > \Omega_{+-}^0 > \Omega_{++}^0 > 0$ and $\Omega_{--}^M > \Omega_{+-}^M > 0 > \Omega_{++}^M$. These results demonstrate that the experimentally observed negative transference number in PEO-LiTFSI systems is captured with the present force field parameterization used in the MD simulations.

If looking at the effects of RF, we see that Ω_{--} and Ω_{+-} changes more significantly upon RF transformation, as compared to Ω_{++} . Especially, at $r = 0.15$, Ω_{+-}^M is negative while Ω_{+-}^0 is positive. This means that the driving force applied to the cations correlates to a co-directional anion flux in the solvent-fixed RF, but that an opposite anion flux is found in the barycentric RF. This, together with the observations made above, cannot be explained by any distribution of ideal charge carrying clusters.

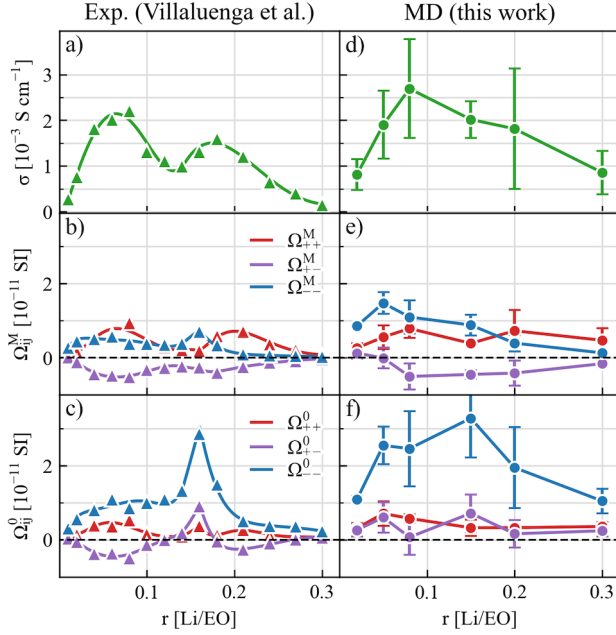


Figure 3. Ionic conductivity and Onsager coefficients under the barycentric and solvent-fixed derived from a-c) experimental measurements and d-f) MD simulations. The experimental measurements (triangle dots) and fittings (curved lines) are taken from Ref. 8. The MD simulation results are computed by fitting the mean displacement correlations functions, as detailed in the Supporting Information.

To better understand the underlying physical account, we can look into the Onsager coefficients from a microscopic point of view, as they are related to the correlations functions of the fluxes. From the equations shown below, it is clear that the RF transformation is equivalent to transforming either the current-correlation function shown in Eq. 8 or, equivalently, the displacements of ions shown in Eq. 9. Thus, this result (Eq. 10) is consistent with Eq. 7, and Wheeler and Newman’s expression for Ω_{ij}^0 .²⁵

$$\Omega_{ij}^0 = \frac{\beta}{3} \int d\mathbf{r} \int_0^\infty dt \langle \mathbf{J}_i^0(0,0) \cdot \mathbf{J}_j^0(\mathbf{r},t) \rangle \quad (8)$$

$$= \lim_{t \rightarrow \infty} \frac{\beta}{6VN_A^2 t} \langle \Delta \mathbf{r}_i^0(t) \cdot \Delta \mathbf{r}_j^0(t) \rangle \quad (9)$$

$$= \lim_{t \rightarrow \infty} \frac{\beta}{6VN_A^2 t} \left\langle \left(\sum_k A_{ik}^{0M} \Delta \mathbf{r}_k^M(t) \right) \cdot \left(\sum_l A_{jl}^{0M} \Delta \mathbf{r}_l^M(t) \right) \right\rangle \quad (10)$$

where $\beta = 1/(k_B T)$ is the inverse temperature, N_A is the Avogadro constant and $\Delta \mathbf{r}_i^R(t)$ is the total displacement of species i over a time interval t .

Based on this result, the conversion of Onsager coefficients upon an RF transformation can be visualized as an affine transformation of ion displacement, as shown in Fig. 4. At $r = 0.15$, the displacement of cations and anions are apparently anti-correlated in the barycentric RF, while the correlation becomes positive in the solvent-fixed RF. This can be rationalized, since the motion of anions in the barycentric RF entails the motion of solvent in the opposite direction, giving rise to the enhanced anion motion and the positive cation-anion correlation in the solvent-fixed RF. On the other hand, the motion of cations induces a much less significant effect, as signified by the small distortion along the

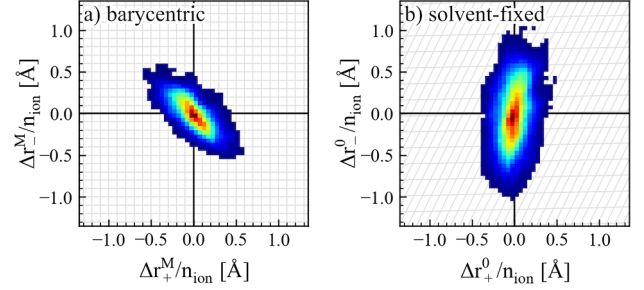


Figure 4. Transformation of the normalized displacement correlations upon a change of reference frame. $\Delta r^M/n_{ion}$ is the total displacement Δr^M (of cations “+” or anions “-”) normalized by the number of ions n_{ion} . The correlation is obtained from a 400 ns MD trajectory, where the correlation between mean displacements of cations and anions over $\Delta t=10$ ns is plotted in a) the barycentric RF and b) the solvent-fixed RF. The RF transformation according to Eq. 7 is visualized as the projection of grid lines from a) to b).

x-axis. This points in the direction that anions play a significant role for the transference number of Li^+ , not only by its relative motion to the cation.

Indeed, the sign of the experimentally measured t_+^0 depends not only on $\Omega_{++}^M - \Omega_{+-}^M$, as is evident in Eq. 3, but also on the Ω_{--}^M and the anion mass fraction. The importance of the anion-anion correlation and the anion mass is demonstrated in Fig. 5, where the partial derivative of t_+^0 shows its strong dependency on the anion mass and Onsager coefficients. An increase of the anion mass introduces an even stronger reduction of the transference number t_+^0 , and therefore t_+^0 is more likely to be negative. The same effect occurs when the anion-anion correlation becomes stronger and Ω_{--}^M becomes larger. This suggests a direct connection between the observed negative t_+^0 and a strong anion-anion correlation found at higher concentrations. The latter effect was also indicated in a recent X-ray scattering study of PEO-LiTFSI systems.¹²

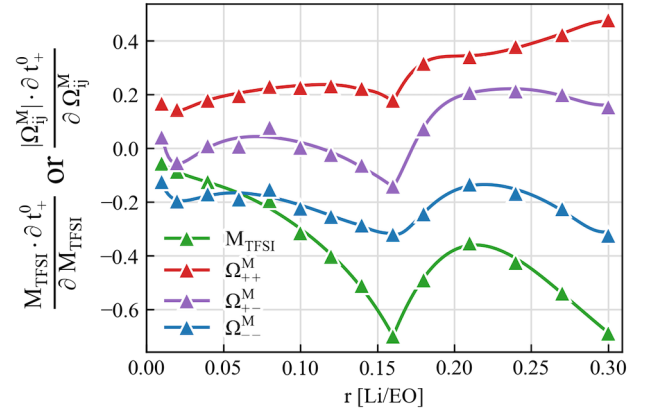


Figure 5. The sensitivity of transference number t_+^0 in solvent-fixed RF to the variations in the anion molecular weight M_{TFSI} and different Onsager coefficients Ω_{ij}^M in the barycentric RF. The analysis is done by evaluating the partial derivative of t_+^0 to the logarithm of M_{TFSI} or $|\Omega_{ij}^M|$, with data derived from experimental measurements in Ref. 8. Note that Ω_{+-}^M is mostly negative as shown in Fig. 3, while the other variables are positive.

In summary, our present analysis reveals a strong RF dependency of the transference number and the Onsager coefficients in the PEO-LiTFSI system. With a proper trans-

formation, the Onsager coefficients can be used as a rigorous test to compare the transport properties from experimental measurements and MD simulations, as shown here. This will provide a new ground to refine force field parameterization, for example, by including the subtle effects of electronic polarization,²⁶ although we found that the standard force field already captures the main features observed in experiments.

Not only do our results demonstrate that the experimentally observed negative t_+^0 can be reproduced with MD simulations, but they also show that cations and anions are anti-correlated in the barycentric RF ($\Omega_{+-}^M < 0$) throughout the entire concentration range in both experiment and simulation. While this does not rule out the possibility of short-lived ion aggregates, neither does it support a transport mechanism based on negatively-charged ion clusters. Instead, we show that a large anion mass and strong anion-anion correlations can be responsible for a negative transference number of t_+^0 .

Furthermore, the RF-dependence of ion-ion correlations suggests that any discussions about ion-ion correlations need to be done within the same RF. This may shed light on why a different observation was made regarding the sign of t_+ with alternative experimental approaches such as electrophoretic NMR (eNMR).¹⁰

Although we do not expect that all discrepancies in transport properties between different experimental approaches and between experiment and simulation can be resolved by the present analysis, insights regarding the RF dependency of ion-ion correlations, and direct comparison of the complete set of Onsager coefficients between experiment and simulation as demonstrated in this work would be essential to elucidate the ion transport mechanism in polymer electrolytes and alike concentrated electrolyte systems.

Acknowledgement This work has been supported by the European Research Council (ERC), grant no. 771777 “FUN POLYSTORE” and the Swedish Research Council (VR), grant no. 2019-05012. The authors thanks funding from the Swedish National Strategic e-Science program eSSSENCE, STandUP for Energy and BASE (Batteries Sweden). The simulations were performed on the resources provided by the Swedish National Infrastructure for Computing (SNIC) at PDC.

Supporting Information Available

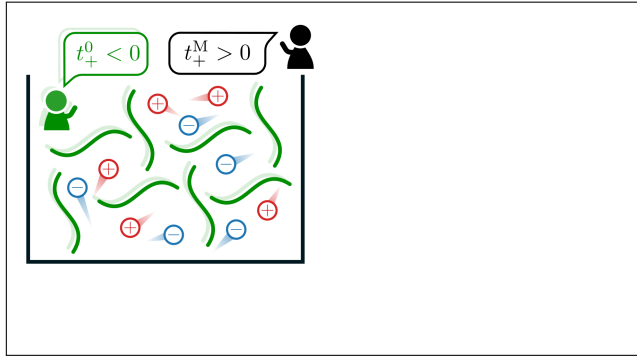
Details of MD simulations and force field parameters; Computation and conversion of Onsager coefficients in different RFs; Conversion between different sets of transport equations; List of symbols.

References

- (1) Mindemark, J.; Lacey, M. J.; Bowden, T.; Brandell, D. Beyond PEO—Alternative host materials for Li^+ -conducting solid polymer electrolytes. *Prog. Polym. Sci.* **2018**, *81*, 114–143.
- (2) Choo, Y.; Halat, D. M.; Villaluenga, I.; Timachova, K.; Balsara, N. P. Diffusion and migration in polymer electrolytes. *Prog. Polym. Sci.* **2020**, *103*, 101220.
- (3) Evans, J.; Vincent, C. A.; Bruce, P. G. Electrochemical measurement of transference numbers in polymer electrolytes. *Polymer* **1987**, *28*, 2324–2328.
- (4) Bruce, P. G.; Vincent, C. A. Steady state current flow in solid binary electrolyte cells. *J. Electroanal. Chem. Interfacial Electrochem.* **1987**, *225*, 1–17.

- (5) Newman, J.; Balsara, N. P. *Electrochemical Systems*; Wiley, 2020.
- (6) Miller, D. G. Application of Irreversible Thermodynamics to Electrolyte Solutions. I. Determination of Ionic Transport Coefficients l_{ij} for Isothermal Vector Transport Processes in Binary Electrolyte Systems. *J. Phys. Chem.* **1966**, *70*, 2639–2659.
- (7) Zwanzig, R. Time-Correlation Functions and Transport Coefficients in Statistical Mechanics. *Annu. Rev. Phys. Chem.* **1965**, *16*, 67–102.
- (8) Villaluenga, I.; Pesko, D. M.; Timachova, K.; Feng, Z.; Newman, J.; Srinivasan, V.; Balsara, N. P. Negative Stefan-Maxwell Diffusion Coefficients and Complete Electrochemical Transport Characterization of Homopolymer and Block Copolymer Electrolytes. *J. Electrochem. Soc.* **2018**, *165*, A2766–A2773.
- (9) Hoffman, Z. J.; Shah, D. B.; Balsara, N. P. Temperature and concentration dependence of the ionic transport properties of poly(ethylene oxide) electrolytes. *Solid State Ion.* **2021**, *370*, 115751.
- (10) Rosenwinkel, M. P.; Schönhoff, M. Lithium Transference Numbers in PEO/LiTFSI Electrolytes Determined by Electrophoretic NMR. *J. Electrochem. Soc.* **2019**, *166*, A1977–A1983.
- (11) Molinari, N.; Mailoa, J. P.; Kozinsky, B. Effect of Salt Concentration on Ion Clustering and Transport in Polymer Solid Electrolytes: A Molecular Dynamics Study of PEO–LiTFSI. *Chem. Mater.* **2018**, *30*, 6298–6306.
- (12) Loo, W. S.; Fang, C.; Balsara, N. P.; Wang, R. Uncovering Local Correlations in Polymer Electrolytes by X-ray Scattering and Molecular Dynamics Simulations. *Macromolecules* **2021**, *54*, 6639–6648.
- (13) France-Lanord, A.; Grossman, J. C. Correlations from Ion Pairing and the Nernst-Einstein Equation. *Phys. Rev. Lett.* **2019**, *122*, 136001.
- (14) Woolf, L. A.; Harris, K. R. Velocity correlation coefficients as an expression of particle-particle interactions in (electrolyte) solutions. *J. Chem. Soc., Faraday Trans. 1* **1978**, *74*, 933–947.
- (15) Vargas-Barbosa, N. M.; Roling, B. Dynamic Ion Correlations in Solid and Liquid Electrolytes: How Do They Affect Charge and Mass Transport? *ChemElectroChem* **2020**, *7*, 367–385.
- (16) Zhang, Z.; Wheatle, B. K.; Krajniak, J.; Keith, J. R.; Ganesan, V. Ion Mobilities, Transference Numbers, and Inverse Haven Ratios of Polymeric Ionic Liquids. *ACS Macro Lett.* **2020**, *9*, 84–89.
- (17) Pfeifer, S.; Ackermann, F.; Sälzer, F.; Schönhoff, M.; Roling, B. Quantification of cation–cation, anion–anion and cation–anion correlations in Li salt/glyme mixtures by combining very-low-frequency impedance spectroscopy with diffusion and electrophoretic NMR. *Phys. Chem. Chem. Phys.* **2021**, *23*, 628–640.
- (18) Fong, K. D.; Self, J.; McCloskey, B. D.; Persson, K. A. Ion Correlations and Their Impact on Transport in Polymer-Based Electrolytes. *Macromolecules* **2021**, *54*, 2575–2591.
- (19) Gudla, H.; Shao, Y.; Phunnarungsri, S.; Brandell, D.; Zhang, C. Importance of the Ion-Pair Lifetime in Polymer Electrolytes. *J. Phys. Chem. Lett.* **2021**, *12*, 8460–8464.
- (20) Onsager, L. Theories and problems of liquid diffusion. *Ann. N. Y. Acad. Sci.* **1945**, *46*, 241–265.
- (21) Kirkwood, J. G.; Baldwin, R. L.; Dunlop, P. J.; Gosting, L. J.; Kegeles, G. Flow Equations and Frames of Reference for Isothermal Diffusion in Liquids. *J. Chem. Phys.* **1960**, *33*, 1505–1513.
- (22) Miller, D. G. Some comments on multicomponent diffusion: negative main term diffusion coefficients, second law constraints, solvent choices, and reference frame transformations. *J. Phys. Chem.* **1986**, *90*, 1509–1519.
- (23) Abraham, M. J.; Murtola, T.; Schulz, R.; Páll, S.; Smith, J. C.; Hess, B.; Lindahl, E. GROMACS: High performance molecular simulations through multi-level parallelism from laptops to supercomputers. *SoftwareX* **2015**, *1–2*, 19–25.
- (24) Wang, J.; Wolf, R. M.; Caldwell, J. W.; Kollman, P. A.; Case, D. A. Development and testing of a general amber force field. *J. Comput. Chem.* **2004**, *25*, 1157–1174.
- (25) Wheeler, D. R.; Newman, J. Molecular Dynamics Simulations of Multicomponent Diffusion. 1. Equilibrium Method. *J. Phys. Chem. B* **2004**, *108*, 18353–18361.
- (26) Borodin, O. Polarizable Force Field Development and Molecular Dynamics Simulations of Ionic Liquids. *J. Phys. Chem. B* **2009**, *113*, 11463–11478.

Graphical TOC Entry



Supporting Information:

Transference Number in Polymer Electrolytes:

Mind the Reference-frame Gap

Yunqi Shao, Harish Gudla, Daniel Brandell, and Chao Zhang*

*Department of Chemistry-Ångström Laboratory, Uppsala University, Lägerhyddsvägen 1, P.
O. Box 538, 75121 Uppsala, Sweden*

E-mail: chao.zhang@kemi.uu.se

MD simulations and force field parameters

The General AMBER force field (GAFF)^{S1} parameters were used for describing bonding and non-bonding interactions in PEO and LiTFSI. The force field parameters along with atomic partial charges were obtained and assigned using ACPYPE^{S2} and ANTECHAMBER^{S3} tools. These partial charges on the salt were scaled by a factor of 0.75 to effectively introduce electronic polarizations and also previously shown to better reproduce experimental diffusivities.

Table S1: The atomic partial charges of PEO and LiTFSI from GAFF.

PEO		LiTFSI	
Atom type	Charge (e)	Atom type	Charge (e)
C	0.130	C	0.417
O _{chain}	-0.429	S	1.113, 1.261
H _{chain}	0.043	F	-0.204
O _{end}	-0.612	N	-0.794
H _{end}	0.405	O	-0.485
		Li	0.750

The initial polymer MD simulation boxes comprising 200 hydroxyl-terminated poly(ethylene oxide) (PEO) chains, each with 25 monomer units (1.11 kg/mol) were constructed using PACKMOL package.^{S4} Six different salt concentrations were obtained by adding 100, 250, 400, 750, 1000 and 1500 lithium bis(trifluoromethane)sulfonimide (LiTFSI) molecules, corresponding to a [Li/EO] concentration ratio of 0.02, 0.05, 0.08, 0.15, 0.20, and 0.3, respectively. After the energy minimization step, all systems were equilibrated first with NVT (constant number of particles, volume, and temperature) and then NPT (constant number of particles, pressure, and temperature) runs using Bussi-Donadio-Parrinello^{S5} thermostat and a Parrinello-Rahman barostat^{S6} at 400 K and 1 bar with a time step of 1 fs. The thermostat and barostat coupling constants were set to 0.1 and 2.0 ps, respectively. Then, NPT production runs were carried out for additional 400 ns at 430K to ensure that the Li-ion dynamics has reached diffusive regime and trajectories were saved every 5 ps.

Computation and conversion of Onsager coefficients in different RFs

The Onsager coefficients from MD simulations are computed with the mean displacement correlations (in the barycentric RF):

$$\Omega_{ij}^M = \lim_{t \rightarrow \infty} \frac{\beta}{6VN_A^2 t} \langle \Delta \mathbf{r}_i^M(t) \cdot \Delta \mathbf{r}_j^M(t) \rangle \quad (\text{S1})$$

where β is the inverse temperature, N_A is the Avogadro constant and $\Delta \mathbf{r}_i^M(t)$ is the total displacement of species i over a time interval t . The limit is estimated by fitting the correlation $\langle \Delta \mathbf{r}_i^M(t) \cdot \Delta \mathbf{r}_j^M(t) \rangle$ as a linear function of t over the interval 10-20ns. The MD trajectories were split into segments of 100ns, and the limit was estimated separately for each segment, where the standard deviation across segments is taken as the error estimation in the main text.

The experimental values of Onsager coefficients for an electrolyte solution of the molar concentration c are computed from the measured conductivity σ , solvent-fixed cation transference number t_+^0 , salt diffusion coefficients D_{salt} , and the so-called thermodynamic factor $1 + \frac{d \ln \gamma_{\pm}}{d \ln m}$:

$$\Omega_{ij}^0 = \frac{t_i^0 t_j^0 \sigma}{z_i z_j F^2} + \frac{c D_{\text{salt}}}{2RT \left(1 + \frac{d \ln \gamma_{\pm}}{d \ln m} \right)} \quad (\text{S2})$$

which is equivalent to that derived by Miller.^{S7} A special form of Eq. 7 in the main text is used to convert the Onsager coefficients for 1:1 electrolytes to solve Ω_{ij}^M from Ω_{ij}^0 or vice versa. Written as the linear relation between independent sets of Ω_{ij} , one have:

$$\begin{bmatrix} \Omega_{++}^0 \\ \Omega_{+-}^0 \\ \Omega_{--}^0 \end{bmatrix} = \frac{1}{\rho_0^2} \begin{bmatrix} (\rho_0 + \rho_+)^2 & 2\rho_-(\rho_0 + \rho_+) & \rho_-^2 \\ \rho_+(\rho_0 + \rho_+) & \rho_0^2 + \rho_0\rho_+ + \rho_0\rho_- + 2\rho_+\rho_- & \rho_-(\rho_0 + \rho_-) \\ \rho_+^2 & 2\rho_+(\rho_0 + \rho_-) & (\rho_0 + \rho_-)^2 \end{bmatrix} \begin{bmatrix} \Omega_{++}^M \\ \Omega_{+-}^M \\ \Omega_{--}^M \end{bmatrix} \quad (\text{S3})$$

where ρ_0 , ρ_+ , ρ_- are the mass concentration of the solvent, the cation, and the anion.

Conversion between different sets of transport equations

In the Maxwell-Stefan equations,^{S8} the driving force is related to relative velocities between different species through the Maxwell-Stefan diffusion coefficients \mathfrak{D}_{ij} or the friction coefficients K_{ij} :

$$c_i \nabla \mu_i = RT \sum_{j \neq i} \frac{c_i c_j}{c_T \mathfrak{D}_{ij}} (\mathbf{v}_j - \mathbf{v}_i) \quad (\text{S4})$$

$$c_i \nabla \mu_i = \sum_{j \neq i} K_{ij} (\mathbf{v}_j - \mathbf{v}_i) \quad (\text{S5})$$

where $c_T = \sum_i c_i$. It follows that K_{ij} and \mathfrak{D}_{ij} are related as:

$$\frac{RT}{\mathfrak{D}_{ij}} = \frac{c_T}{c_i c_j} K_{ij} \quad (\text{S6})$$

The relation between the Maxwell-Stefan coefficients with the Onsager coefficients can be shown through the modified form of Maxwell-Stefan equations introduced by Newman,^{S9} where the relative velocities are replaced with the velocities in the solvent-fixed RF:

$$c_i \nabla \mu_i = \sum_{j \neq 0} M_{ij} (\mathbf{v}_j - \mathbf{v}_0) \quad (\text{S7})$$

M_{ij} are related to K_{ij} as:

$$\begin{bmatrix} K_{+0} \\ K_{+-} \\ K_{-0} \end{bmatrix} = \begin{bmatrix} -1 & -1 & 0 \\ 0 & 1 & 0 \\ 0 & -1 & -1 \end{bmatrix} \begin{bmatrix} M_{++} \\ M_{+-} \\ M_{--} \end{bmatrix} \quad (\text{S8})$$

Inspecting Eq. S7 and the Onsager equations in the solvent-fixed RF (note that $\Omega_{i0}^0 = 0$):

$$\mathbf{J}_i^0 = c_i (\mathbf{v}_j - \mathbf{v}_0) = - \sum_{j \neq 0} \Omega_{ij}^0 \nabla \mu_j \quad (\text{S9})$$

It is clear that the M_{ij} and Ω_{ij}^0 are related with the matrix inversion of transport coefficients, for 1:1 electrolyte solution with concentration c :

$$\begin{bmatrix} M_{++} & M_{+-} \\ M_{+-} & M_{--} \end{bmatrix} = -c^2 \begin{bmatrix} \Omega_{++}^0 & \Omega_{+-}^0 \\ \Omega_{+-}^0 & \Omega_{--}^0 \end{bmatrix}^{-1} \quad (\text{S10})$$

or:

$$\begin{bmatrix} M_{++} \\ M_{+-} \\ M_{--} \end{bmatrix} = \frac{c^2}{\det(\mathbf{\Omega})} \begin{bmatrix} -\Omega_{--}^0 \\ \Omega_{+-}^0 \\ -\Omega_{++}^0 \end{bmatrix} \quad (\text{S11})$$

with:

$$\det(\mathbf{\Omega}) = \Omega_{++}^0 \Omega_{--}^0 - (\Omega_{+-}^0)^2 \quad (\text{S12})$$

$$= \frac{c\sigma D_{\text{salt}}}{2RTF^2 \left(1 + \frac{d \ln \gamma_{\pm}}{d \ln m}\right)} \quad (\text{S13})$$

The consistency between the different sets of transport coefficients may be shown by representing \mathfrak{D}_{ij} in terms of Ω_{ij}^0 :

$$\mathfrak{D}_{+0} = \frac{c_0 RT}{c_T c} \cdot \frac{\det(\mathbf{\Omega})}{\Omega_{--}^0 - \Omega_{+-}^0} \quad (\text{S14})$$

$$\mathfrak{D}_{+-} = \frac{RT}{c_T} \cdot \frac{\det(\mathbf{\Omega})}{\Omega_{+-}^0} \quad (\text{S15})$$

$$\mathfrak{D}_{-0} = \frac{c_0 RT}{c_T c} \cdot \frac{\det(\mathbf{\Omega})}{\Omega_{++}^0 - \Omega_{+-}^0} \quad (\text{S16})$$

Combining Eq. S14-S16 and Eq. S2, we arrived at the same relation between \mathfrak{D}_{ij} and experimental measurables, as is studied in Ref. S10 and S11, which proves the consistency

between different descriptions of transport coefficients.

$$\mathfrak{D}_{+0} = \frac{c_0 D_{\text{salt}}}{2c_T t_-^0 \left(1 + \frac{d \ln \gamma_{\pm}}{d \ln m}\right)} \quad (\text{S17})$$

$$\mathfrak{D}_{+-} = \left[\frac{c_T F^2}{\sigma R T} - \frac{2t_+^0 t_-^0 \left(1 + \frac{d \ln \gamma_{\pm}}{d \ln m}\right)}{c D} \right]^{-1} \quad (\text{S18})$$

$$\mathfrak{D}_{-0} = \frac{c_0 D_{\text{salt}}}{2c_T t_+^0 \left(1 + \frac{d \ln \gamma_{\pm}}{d \ln m}\right)} \quad (\text{S19})$$

List of symbols

a_i^S	weighing factor of species i under reference frame S
A_{ij}^{RS}	matrix elements to convert the independent fluxes from reference frame S to R
c	salt concentration
c_i	molar concentration of species i
c_T	total solution concentration
D_{salt}	salt diffusion coefficient
\mathfrak{D}_{ij}	Maxwell-Stefan diffusion coefficient for interaction of species i and j
F	Faraday's constant
\mathbf{J}_i^S	flux of species i under reference frame S
k_B	Boltzmann constant
K_{ij}	friction coefficient for interaction of species i and j
m	molality
M_{ij}	modified friction coefficient for interaction of species i and j
M_i	molecular weight of species i
n_{ion}	number of ions (cation or anion)
N_A	Avogadro constant
q_i	formal charge of species i
r	salt concentration ratio [Li/EO]
\mathbf{r}_i^S	summed coordinate vector of species i under reference frame S
R	gas constant
t	time interval
t_i^S	transference number of species i under reference frame S
T	temperature
\mathbf{v}_i	mean velocity of species i
\mathbf{X}_i	external driving force on species i
z_i	charge number of species i

γ_{\pm}	mean molal activity coefficient of the salt
δ_{ij}	Kronecker delta function for interaction of species i and j
μ_i	mobility of species i
ρ	density
ρ_i	mass concentration of species i
σ	total ionic conductivity
β	inverse temperature
ω_i	mass fraction of species i
Ω_{ij}^S	Onsager coefficient for interaction of species i and j under reference frame S

References

- (S1) Wang, J.; Wolf, R. M.; Caldwell, J. W.; Kollman, P. A.; Case, D. A. Development and testing of a general amber force field. *J. Comput. Chem.* **2004**, *25*, 1157–1174.
- (S2) Sousa Da Silva, A. W.; Vranken, W. F. ACPYPE - AnteChamber PYthon Parser interface. *BMC Res. Notes* **2012**, *5*, 367.
- (S3) Wang, J.; Wang, W.; Kollman, P. A.; Case, D. A. Automatic atom type and bond type perception in molecular mechanical calculations. *J. Mol. Graph. Model.* **2006**, *25*, 247–260.
- (S4) Martínez, L.; Andrade, R.; Birgin, E. G.; Martínez, J. M. Packmol: A Package for Building Initial Configurations for Molecular Dynamics Simulations. *J. Comput. Chem.* **2009**, *30*, 2157–2164.
- (S5) Bussi, G.; Donadio, D.; Parrinello, M. Canonical sampling through velocity rescaling. *J. Chem. Phys.* **2007**, *126*, 014101.
- (S6) Parrinello, M.; Rahman, A. Polymorphic transitions in single crystals: A new molecular dynamics method. *J. Appl. Phys.* **1981**, *52*, 7182–7190.
- (S7) Miller, D. G. Application of Irreversible Thermodynamics to Electrolyte Solutions. I. Determination of Ionic Transport Coefficients l_{ij} for Isothermal Vector Transport Processes in Binary Electrolyte Systems. *J. Phys. Chem.* **1966**, *70*, 2639–2659.
- (S8) Krishna, R.; Wesselingh, J. The Maxwell-Stefan approach to mass transfer. *Chem. Eng. Sci.* **1997**, *52*, 861–911.
- (S9) Wheeler, D. R.; Newman, J. Molecular Dynamics Simulations of Multicomponent Diffusion. 1. Equilibrium Method. *J. Phys. Chem. B* **2004**, *108*, 18353–18361.

- (S10) Balsara, N. P.; Newman, J. Relationship between Steady-State Current in Symmetric Cells and Transference Number of Electrolytes Comprising Univalent and Multivalent Ions. *J. Electrochem. Soc.* **2015**, *162*, A2720–A2722.
- (S11) Villaluenga, I.; Pesko, D. M.; Timachova, K.; Feng, Z.; Newman, J.; Srinivasan, V.; Balsara, N. P. Negative Stefan-Maxwell Diffusion Coefficients and Complete Electrochemical Transport Characterization of Homopolymer and Block Copolymer Electrolytes. *J. Electrochem. Soc.* **2018**, *165*, A2766–A2773.